

Article

Demonstration of a Compact Magneto-Optical Trap on an Unstaffed Aerial Vehicle

Luuk Earl ¹, Jamie Vovrosh ¹, Michael Wright ^{1,2}, Daniel Roberts ³, Jonathan Winch ¹, Marisa Perea-Ortiz ¹, Andrew Lamb ¹, Farzad Hayati ¹, Paul Griffin ², Nicole Metje ³, Kai Bongs ¹ and Michael Holyński ^{1,*}

¹ Midlands Ultracold Atom Research Centre, School of Physics and Astronomy, University of Birmingham, Birmingham B15 2TT, UK; luukearl@hotmail.co.uk (L.E.); j.a.vovrosh@bham.ac.uk (J.V.); michael.wright@strath.ac.uk (M.W.); j.winch.1@bham.ac.uk (J.W.); marisa.pereaortiz@gmail.com (M.P.-O.); a.a.lamb.1@bham.ac.uk (A.L.); f.hayati@bham.ac.uk (F.H.); k.bongs@bham.ac.uk (K.B.)

² Scottish Universities Physics Alliance and Department of Physics, University of Strathclyde, Glasgow G4 0NG, UK; paul.griffin@strath.ac.uk

³ School of Engineering, University of Birmingham, Birmingham B15 2TT, UK; dlr677@student.bham.ac.uk (D.R.); n.metje@bham.ac.uk (N.M.)

* Correspondence: M.Holynski@bham.ac.uk; Tel.: +44-1214148303

Abstract: The extraordinary performance offered by cold atom-based clocks and sensors has the opportunity to profoundly affect a range of applications, for example in gravity surveys, enabling long term monitoring applications through low drift measurements. While ground-based devices are already starting to enter the commercial market, significant improvements in robustness and reductions to size, weight, and power are required for such devices to be deployed by Unstaffed Aerial Vehicle systems (UAV). In this article, we realise the first step towards the deployment of cold atom based clocks and sensors on UAV's by demonstrating an UAV portable magneto-optical trap system, the core package of cold atom based systems. This system is able to generate clouds of $2.1 \pm 0.2 \times 10^7$ atoms, in a package of 370 mm × 350 mm × 100 mm, weighing 6.56 kg, consuming 80 W of power.

Keywords: quantum technology; cold atoms; magneto-optical trap; atom interferometry; unstaffed aerial vehicle



Citation: Earl, L.; Vovrosh, J.; Wright, M.; Roberts, D.; Winch, J.; Perea-Ortiz, M.; Lamb, A.; Hayati, F.; Griffin, P.; Metje, N.; et al. Demonstration of a Compact Magneto-Optical Trap on an Unstaffed Aerial Vehicle. *Atoms* **2022**, *10*, 32. <https://doi.org/10.3390/atoms10010032>

Academic Editor: Gordon W.F. Drake

Received: 28 January 2022

Accepted: 15 March 2022

Published: 17 March 2022

Publisher's Note: MDPI stays neutral with regard to jurisdictional claims in published maps and institutional affiliations.



Copyright: © 2022 by the authors. Licensee MDPI, Basel, Switzerland. This article is an open access article distributed under the terms and conditions of the Creative Commons Attribution (CC BY) license (<https://creativecommons.org/licenses/by/4.0/>).

1. Introduction

Quantum technology based on cold atoms [1] has proven to be a powerful method for precision sensing [2,3] and time keeping [4]. For example, within laboratories, cold atom sensors have provided sensitive measurements of gravity [5], enabling investigations of the equivalence principle [6], the fine-structure constant [7], and Newton's gravitational constant [8], as well as prompting the desire to transition these sensors into practical devices for use in real-world environments [2]. Currently, cold atom-based sensors have been demonstrated in urban [9] and mountainous environments [10,11], on road vehicles [12], aircraft [13,14], ships [15], the International Space Station [16], and on rockets [17].

There is significant interest in developing such systems for small and remote, or autonomous, platforms that require compact sensors. In particular, the deployment of sensors using Unstaffed Aerial Vehicles (UAVs) would enable applications that require access to inaccessible or hazardous locations—and future operation in flight on UAVs may enable autonomous surveillance and a wide range of applications. UAVs are used in a number of applications including archaeology [18], disaster recovery [19], forestry research [20], precision agriculture [21], and detection of rift basins [22]. Adding cold atom-based sensing to the array of sensors already deployed by and available on UAVs would not only enhance existing applications, but has the potential to open up new ones [2,23]. However, before wide adoption of cold atom based sensors and clocks can be realised, a

number of challenges need to be overcome, including strict Size, Weight, and Power (SWaP) requirements and robustness against platform motion.

This article presents the first step towards a UAV portable cold atom device, by demonstrating a compact Magneto-Optical Trap (MOT) capable of being moved and deployed by a UAV, as well as demonstrating its operation during flight.

2. System Overview

The compact MOT system can be seen in Figure 1 and contains all the electronic, vacuum, and laser components required to generate a MOT.

The ultra-high vacuum environment is maintained within the science chamber by an active ion pump and passive getter pump when not in flight, and just the unpowered getter pump while in flight. When actively pumping, the chamber is maintained at an equilibrium pressure of 4×10^{-9} mbar. The vacuum system houses rubidium dispensers which generate a background gas from which the MOT can load, in addition to four 10 mm prisms, a mirror, and a quarter wave plate arranged such that the beams required for laser cooling can be generated from a single input telescope [24,25]. The science chamber is shown in Figure 1B.

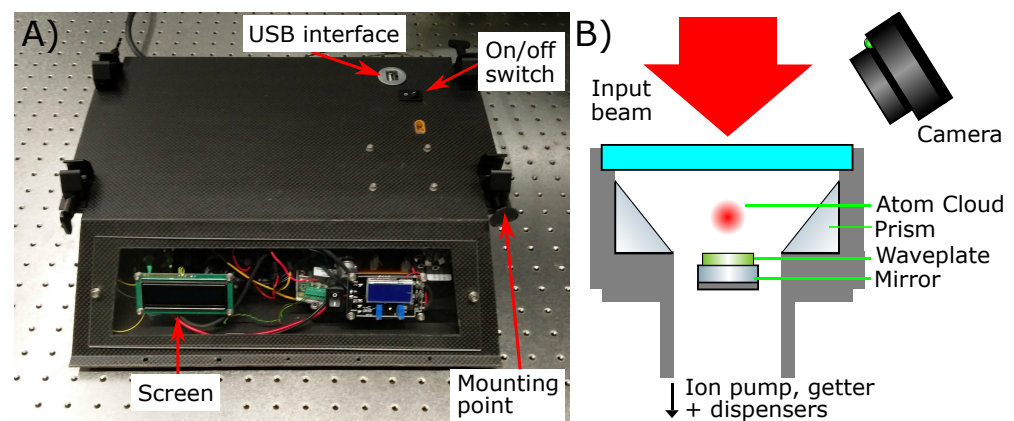


Figure 1. (A) The compact MOT system, which is contained within a custom light weight carbon fibre enclosure with dimensions of $370 \text{ mm} \times 350 \text{ mm} \times 100 \text{ mm}$. (B) Schematic of the custom titanium science chamber in which the atom cloud is formed. The science chamber design is similar to that in reference [26]. A camera off axis to the input beam is used to observe the MOT through the same window as the input beam.

The quadrupole magnetic field environment required by the MOT was generated with permanent magnets arranged in a north–south cross configuration [24], with two $3 \text{ mm} \times 3 \text{ mm} \times 8 \text{ mm}$ neodymium magnets at each cross point producing a magnetic field gradient of 17 G/cm . As an alternative, the system can be fitted with a pair of coils that can be used to generate a similar quadrupole field. If used, the coils require 6.4 W of power to operate.

The light used to cool and trap the atoms is generated with a frequency-doubled fibre laser system, a schematic of which can be seen in Figure 2. The use of fibre integrated components alleviates alignment issues, improving resilience against the effects of platform motion, such as mechanical shock and vibration [27]. The two frequencies needed for cooling ^{87}Rb atoms on the D2 transition are derived from the carrier and first-order frequency sideband created by phase modulation. The laser is linearly scanned over a region of 500 MHz to generate the cooling frequency. The laser frequency is scanned using an Arduino microcontroller generating a triangle wave, which scanned the piezo input of the seed laser, passing over half the cooling frequency on the cycling $|F' = 2\rangle \rightarrow |F' = 3\rangle$ transition roughly once every 40 s . The light from the seed laser is passed through an electro-optical modulator (EOM), which modulates the light at 6.5 GHz to generate a sideband that acts as the repumping frequency on the $|F = 1\rangle \rightarrow |F' = 2\rangle$ transition. After

the EOM the light is then amplified with an erbium-doped fibre amplifier (EDFA) before being frequency doubled from 1560 nm to 780 nm in a periodically poled lithium niobate (PPLN) waveguide. The system can produce up to 450 mW of 780 nm laser light at the output into the fibre. The light out of the fibre then passes through a quarter waveplate to produce circularly polarised light and two beam expanders such that when the light reaches the prisms it has a beam diameter of 30 mm ($1/e^2$). When left to run autonomously, the system generates a cloud of atoms lasting roughly 1 s every 40 s. Alternatively, the system could be locked to the fluorescence of the MOT [24].

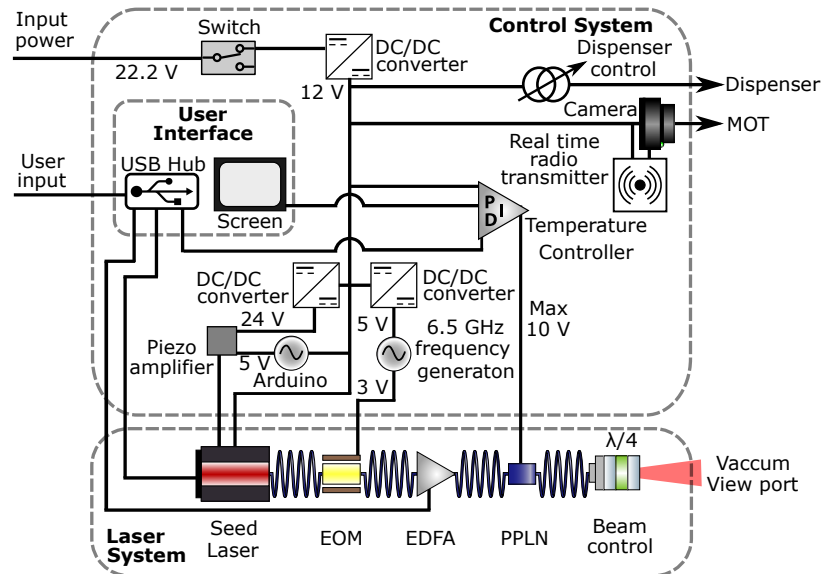


Figure 2. A block diagram of the electrical and optical components in the payload. The 22.2 Volt line from the batteries is fed into the payload; this is then converted into the required powers for each component. The output light from a seed laser (1560 nm) is modulated by an EOM driven by an oscillator to generate frequency sidebands, this is then amplified by a 1 W EDFA before being frequency doubled via second harmonic generation using a PPLN waveguide. The output of the fibre passes through two beam expanders and a quarter waveplate. This light is then input into the MOT vacuum chamber. A user interface allows for users to communicate with various sub-components and monitor the status of the payload. While in flight, the camera feed is broadcast in real time to the operator on the ground.

The laser system and control system are integrated around the vacuum system into a custom carbon fibre enclosure as shown in Figure 3.

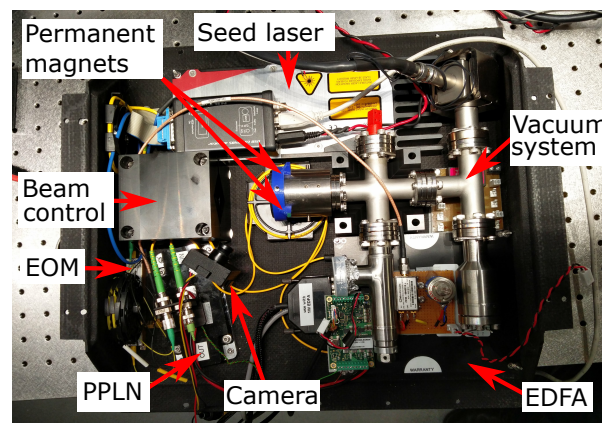


Figure 3. Photo showing the laser system and vacuum system integrated into the carbon fibre enclosure.

The atom number produced in the system was characterised using a MOT loading curve [28]. An example loading curve can be seen in Figure 4. The MOT, when fully loaded, has an atom number of $2.1 \pm 0.2 \times 10^7$ and has a loading time constant of 1.47 ± 0.12 s. This is similar to what is achieved in existing cold atom based sensors [3,10,13,29].

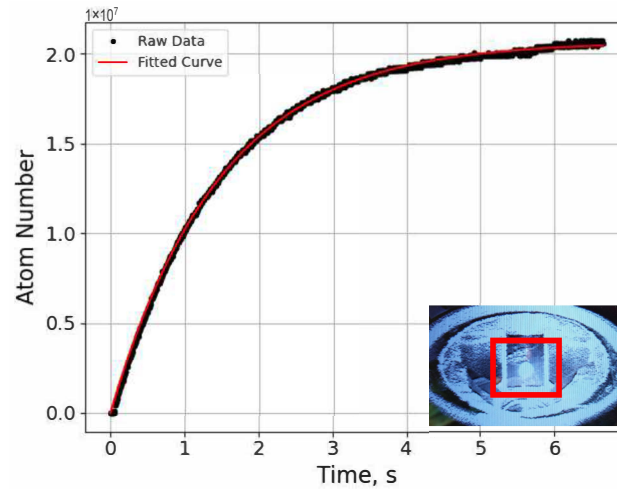


Figure 4. Example MOT loading curve taken while on the ground with the ion pump in operation. The loading curve has been fitted with equation 2 from reference [28]. The inset shows a photo of prism MOT. The atom cloud is highlighted within the red square.

The weight and power consumption when the MOT is running at peak power in flight is shown in Table 1. The majority of the power consumption is by the UAV itself; depending on the environmental factors, such as wind, and the amount of acceleration, the consumption may vary significantly. However, in a calm environment with moderate acceleration, the consumption would remain near the lower end of power range. The power consumption of the compact MOT is dominated by the laser system, in particular the EDFA, which accounts for 37% of the power consumption. The batteries are the heaviest component in the system and account for 28% of the total weight. The total weight of the UAV, compact MOT, and batteries, as well as the total power draw, will limit the total flight time possible with the system; we estimate this to be 18 min, compared to a maximum flight time of 32 min without the compact MOT system. Longer flight times will become possible with further SWaP reductions in cold atom systems; for example, halving the weight of the compact MOT would increase the max total flight time to 26 min. Examples of innovations which could be utilised to produce a SWaP optimised cold atom sensor include compact laser systems [30–32], optimised 3D printed components [33–36], high-flux compact cold-atom sources [37], and passively pumped vacuum cells [38–40].

In addition to implementing SWaP reductions to cold atom systems, implementing existing solutions to increase UAV flight times would enable longer flight times and include integration of a tether for power and data transmission [41], autonomous deployment and recovery from a charging station [42,43], solar-powered photovoltaic panels [44], larger UAVs, and use of batteries with high-power density such as high voltage lithium-ion polymer batteries [45].

Table 1. The weight and power budget of the UAV with the portable compact MOT system in flight. The brackets show the effect of running the system with coils instead of magnets has on the power consumption of the system.

Subsystem	Weight (kg)	Power/Energy
Vacuum Chamber	1.58	15.00 W
Magnetic field generation	0.02	— (6.4 W)
Laser and control system	4.46	65.00 W
Housing and mounting	0.50	—
UAV	7.40	3.00–15.55 kW
Batteries	5.40	977.00 Wh
Total	19.36	3.08–15.63 kW (3.09–15.64 kW)

3. Test Flight

The system was shut-down and transported via car for ~ 45 min to a field in Birmingham, United Kingdom, on 7 March 2017 for a test flight. The compact MOT was mounted to a Vulcan UAV (from Raven UAV Ltd. Mitcheldean, Gloucestershire, UK) along with two Lithium Polymer (LiPo) batteries, which were able to supply 22.2 Volts with 22 Amp-hours of charge. These batteries were used to power both the compact MOT system and the UAV. The system can be seen in Figure 5A. The system was set to generate atom clouds periodically while on the ground and left to run autonomously throughout the whole of the test flight. The system was then flown to a height of ~ 10 m, after which it hovered for 10 min before landing, during which time several atom clouds were generated. The system in flight can be seen in Figure 5B.

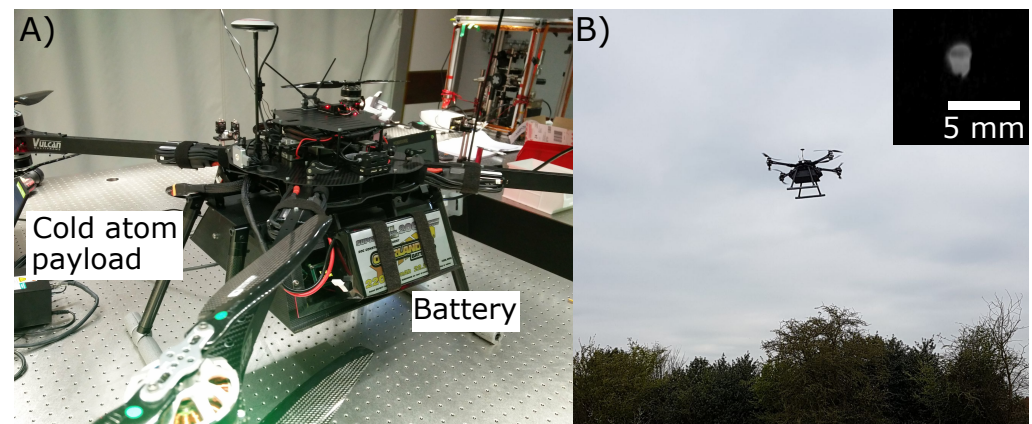


Figure 5. (A) The VulcanUAV Raven complete with (LiPo) batteries and compact MOT payload. (B) The MOT system in flight. The inset shows a photo of an atom cloud generated in the system during flight, after background subtraction.

4. Discussion

The high precision and low-drift measurements offered by cold atom systems, once realised in a UAV portable package, have the opportunity to enhance sensing capability, particularly in a number of hard to reach, inaccessible or hazardous locations (examples include steep sides of volcanoes and dense forests) as well as rapid redeployment in cases of time-varying features for applications such as hydrological monitoring. Furthermore, a future UAV portable system could allow for deployment and redeployment of sensors to enable automated large area surveys, for example in archaeological applications, enabling the detection of tombs or buried cities or used for the mapping of aquifers.

To push cold atom based sensors towards the SWaP profile that is required for deployment and operation on UAVs, the first UAV portable cold atoms system has been developed. This system is capable of generating atom clouds consisting of $2.1 \pm 0.2 \times 10^7$ laser-cooled atoms in a system package of 370 mm \times 350 mm \times 100 mm, weighing 6.56 kg and power consumption of 80 W. The system has successfully shown autonomous operation during a 10 minute flight \sim 10 m above the ground on-board a commercial-off-the-shelf UAV.

To upgrade the demonstrator shown here to a full sensor, additional functionality will need to be implemented, primarily needing extensions to the control and laser system, while meeting the requirements for UAV operation. These requirements can be split into two categories, namely sufficiently small SWaP and robustness to platform motion, both of which are active research areas. For example, for the gravimeter gradiometer in reference [9] to have the same weight, and hence similar flight time, as the MOT demonstrator presented here, it would need to be reduced in weight by a factor of \approx 50 times while having techniques such as those implemented in references [12,13,15] incorporated into the system to allow for measurements while in motion. While there is a clear route to further reduce the SWaP and realise sensing capabilities, achieving a UAV portable MOT is the first step towards achieving cold atom-based sensing on UAVs.

Author Contributions: Conceptualization, M.H.; methodology, L.E.; software, L.E.; validation, L.E. and M.W.; formal analysis, L.E.; investigation, L.E., J.V., J.W., F.H., M.W., D.R., M.P.-O. and A.L.; resources, M.H. and J.W.; data curation, J.V.; writing—original draft preparation, J.V.; writing—review and editing, J.V., L.E., J.W., M.H., J.W., F.H., N.M., A.L., P.G., M.W. and K.B.; visualization, J.V. and L.E.; supervision, M.H., N.M., M.P.-O., K.B. and P.G.; project administration, M.H. and K.B.; and funding acquisition, M.H. and K.B. All authors have read and agreed to the published version of the manuscript.

Funding: We acknowledge support from EPSRC through grants EP/M013294/1 and EP/T001046/1 as part of the UK National Quantum Technologies Programme.

Institutional Review Board Statement: Not applicable.

Informed Consent Statement: Not applicable.

Data Availability Statement: Data available upon request.

Conflicts of Interest: J.V. is acting as a guest editor for the special issue of *Atoms* in which this article is being submitted to. The other authors declare no conflicts of interest.

Abbreviations

The following abbreviations are used in this manuscript:

EDFA	Erbium-Doped Fiber Amplifier
EOM	Electro-Optical Modulator
LiPo	Lithium Polymer
MOT	Magneto Optical Trap
PPLN	Periodically Poled Lithium Niobate
SWaP	Size Weight and Power
UAV	Unstaffed Aerial Vehicle

References

1. Kasevich, M.; Chu, S. Atomic interferometry using stimulated Raman transitions. *Phys. Rev. Lett.* **1991**, *67*, 181–184. [[CrossRef](#)] [[PubMed](#)]
2. Bongs, K.; Holynski, M.; Vovrosh, J.; Bouyer, P.; Condon, G.; Rasel, E.; Schubert, C.; Schleich, W.P.; Roura, A. Taking atom interferometric quantum sensors from the laboratory to real-world applications. *Nat. Rev. Phys.* **2019**, *1*, 731–739. [[CrossRef](#)]
3. Behbood, N.; Martin Ciurana, F.; Colangelo, G.; Napolitano, M.; Mitchell, M.W.; Sewell, R.J. Real-time vector field tracking with a cold-atom magnetometer. *Appl. Phys. Lett.* **2013**, *102*, 173504. [[CrossRef](#)]
4. Wolf, P.; Chapelet, F.; Bize, S.; Clairon, A. Cold Atom Clock Test of Lorentz Invariance in the Matter Sector. *Phys. Rev. Lett.* **2006**, *96*, 060801. [[CrossRef](#)]

5. Dickerson, S.M.; Hogan, J.M.; Sugarbaker, A.; Johnson, D.M.S.; Kasevich, M.A. Multiaxis Inertial Sensing with Long-Time Point Source Atom Interferometry. *Phys. Rev. Lett.* **2013**, *111*, 083001. [[CrossRef](#)]
6. Asenbaum, P.; Overstreet, C.; Kim, M.; Curti, J.; Kasevich, M.A. Atom-Interferometric Test of the Equivalence Principle at the 10^{-12} Level. *Phys. Rev. Lett.* **2020**, *125*, 191101. [[CrossRef](#)]
7. Fray, S.; Weitz, M. Atom-Based Test of the Equivalence Principle. *Space Sci. Rev.* **2009**, *148*, 225–232. [[CrossRef](#)]
8. Fixler, J.B.; Foster, G.T.; McGuirk, J.M.; Kasevich, M.A. Atom Interferometer Measurement of the Newtonian Constant of Gravity. *Science* **2007**, *315*, 74–77. [[CrossRef](#)]
9. Stray, B.; Lamb, A.; Kaushik, A.; Vovrosh, J.; Rodgers, A.; Winch, J.; Hayati, F.; Boddice, D.; Stabrawa, A.; Niggebaum, A.; et al. Quantum sensing for gravity cartography. *Nature* **2022**, *602*, 590–594. [[CrossRef](#)]
10. Wu, X.; Pagel, Z.; Malek, B.S.; Nguyen, T.H.; Zi, F.; Scheirer, D.S.; Müller, H. Gravity surveys using a mobile atom interferometer. *Sci. Adv.* **2019**, *5*, eaax0800. [[CrossRef](#)]
11. Carbone, D.; Antoni-Micollier, L.; Hammond, G.; de Zeeuw van Dalfsen, E.; Rivalta, E.; Bonadonna, C.; Messina, A.; Lautier-Gaud, J.; Toland, K.; Koymans, M.; et al. The NEWTON-g Gravity Imager: Toward New Paradigms for Terrain Gravimetry. *Front. Earth Sci.* **2020**, *8*, 452. [[CrossRef](#)]
12. Guo, J.; Ma, S.; Zhou, C.; Liu, J.; Wang, B.; Pan, D.; Mao, A. Vibration Compensation for a Vehicle-mounted Atom Gravimeter. *Preprints* **2021**, *2021*, 110255. [[CrossRef](#)]
13. Bidel, Y.; Zahzam, N.; Bresson, A.; Blanchard, C.; Cadoret, M.; Olesen, A.V.; Forsberg, R. Absolute airborne gravimetry with a cold atom sensor. *J. Geod.* **2020**, *94*, 20. [[CrossRef](#)]
14. Geiger, R.; Ménoret, V.; Stern, G.; Zahzam, N.; Cheinet, P.; Battelier, B.; Villing, A.; Moron, F.; Lours, M.; Bidel, Y.; et al. Detecting inertial effects with airborne matter-wave interferometry. *Nat. Commun.* **2011**, *2*, 474. [[CrossRef](#)]
15. Bidel, Y.; Zahzam, N.; Blanchard, C.; Bonnain, A.; Cadoret, M.; Bresson, A.; Rouxel, D.; Lequentrec-Lalancette, M.F. Absolute marine gravimetry with matter-wave interferometry. *Nat. Commun.* **2018**, *9*, 627. [[CrossRef](#)]
16. Frye, K.; Abend, S.; Bartosch, W.; Bawamia, A.; Becker, D.; Blume, H.; Braxmaier, C.; Chiow, S.; Efremov, M.A.; Ertmer, W.; et al. The Bose-Einstein Condensate and Cold Atom Laboratory. *EPJ Quantum. Technol.* **2021**, *8*, 1. [[CrossRef](#)]
17. Becker, D.; Lachmann, M.D.; Seidel, S.T.; Ahlers, H.; Dinkelaker, A.N.; Grosse, J.; Hellmig, O.; Müntinga, H.; Schkolnik, V.; Wendrich, T.; et al. Space-borne Bose-Einstein condensation for precision interferometry. *Nature* **2018**, *562*, 391–395. [[CrossRef](#)]
18. Campana, S. Drones in Archaeology. State-of-the-art and Future Perspectives. *Archaeol. Prospect* **2017**, *24*, 275–296. [[CrossRef](#)]
19. Rejeb, A.; Rejeb, K.; Simske, S.; Treiblmaier, H. Humanitarian Drones: A Review and Research Agenda. *Internet Things* **2021**, *16*, 100434. [[CrossRef](#)]
20. Tang, L.; Shao, G. Drone remote sensing for forestry research and practices. *J. For. Res.* **2015**, *26*, 791–797. [[CrossRef](#)]
21. Murrieta-Rico, F.N.; Hernandez-Balbuena, D.; Rodriguez-Quiñonez, J.C.; Petranovskii, V.; Raymond-Herrera, O.; Gurko, A.G.; Mercorelli, P.; Sergiyenko, O.; Lindner, L.; Valdez-Salas, B.; et al. Resolution improvement of accelerometers measurement for drones in agricultural applications. In Proceedings of the IECON 2016—42nd Annual Conference of the IEEE Industrial Electronics Society, Florence, Italy, 23–26 October 2016; pp. 1037–1042. [[CrossRef](#)]
22. Jones, P.C.; Johnson, A.C.; von Frese, R.R.; Corr, H. Detecting rift basins in the Evans Ice Stream region of West Antarctica using airborne gravity data. *Tectonophysics* **2002**, *347*, 25–41. [[CrossRef](#)]
23. Krelina, M. Quantum technology for military applications. *EPJ Quantum. Technol.* **2021**, *8*, 24. [[CrossRef](#)]
24. Hinton, A.; Perea-Ortiz, M.; Winch, J.; Briggs, J.; Freer, S.; Moustoukas, D.; Powell-Gill, S.; Squire, C.; Lamb, A.; Rammeloo, C.; et al. A portable magneto-optical trap with prospects for atom interferometry in civil engineering. *Philos. Trans. R. Soc. Lond. Math. Phys. Eng. Sci.* **2017**, *375*, 20160238. [[CrossRef](#)]
25. Lee, K.I.; Kim, J.A.; Noh, H.R.; Jhe, W. Single-beam atom trap in a pyramidal and conical hollow mirror. *Opt. Lett.* **1996**, *21*, 1177–1179. [[CrossRef](#)]
26. Vovrosh, J.; Earl, L.; Thomas, H.; Winch, J.; Stray, B.; Ridley, K.; Langlois, M.; Bongs, K.; Holynski, M. Reduction of background scattered light in vacuum systems for cold atoms experiments. *AIP Adv.* **2020**, *10*, 105125. [[CrossRef](#)]
27. Carraz, O.; Lienhart, F.; Charrière, R.; Cadoret, M.; Zahzam, N.; Bidel, Y.; Bresson, A. Compact and robust laser system for onboard atom interferometry. *Appl. Phys. B* **2009**, *97*, 405. [[CrossRef](#)]
28. Moore, R.W.G.; Lee, L.A.; Findlay, E.A.; Torralbo-Campo, L.; Bruce, G.D.; Cassettari, D. Measurement of vacuum pressure with a magneto-optical trap: A pressure-rise method. *Rev. Sci. Instrum.* **2015**, *86*, 093108. [[CrossRef](#)]
29. Menoret, V.; Vermeulen, P.; Moigne, N.L.; Bonvalot, S.; Bouyer, P.; Landragin, A.; Desruelle, B. Gravity measurements below 10^{-9} g with a transportable absolute quantum gravimeter. *Sci. Rep.* **2018**, *8*, 12300. [[CrossRef](#)]
30. Theron, F.; Bidel, Y.; Dieu, E.; Zahzam, N.; Cadoret, M.; Bresson, A. Frequency-doubled telecom fiber laser for a cold atom interferometer using optical lattices. *Opt. Commun.* **2017**, *393*, 152–155. [[CrossRef](#)]
31. Luo, Q.; Zhang, H.; Zhang, K.; Duan, X.C.; Hu, Z.K.; Chen, L.L.; Zhou, M.K. A compact laser system for a portable atom interferometry gravimeter. *Rev. Sci. Instrum.* **2019**, *90*, 043104. [[CrossRef](#)]
32. Wu, X.; Zi, F.; Dudley, J.; Bilotta, R.J.; Canoza, P.; Müller, H. Multiaxis atom interferometry with a single-diode laser and a pyramidal magneto-optical trap. *Optica* **2017**, *4*, 1545–1551. [[CrossRef](#)]
33. Vovrosh, J.; Voulazeris, G.; Petrov, P.G.; Zou, J.; Gaber, Y.; Benn, L.; Woolger, D.; Attallah, M.M.; Boyer, V.; Bongs, K.; et al. Additive manufacturing of magnetic shielding and ultra-high vacuum flange for cold atom sensors. *Sci. Rep.* **2018**, *8*, 2023. [[CrossRef](#)]

34. Cooper, N.; Coles, L.; Everton, S.; Maskery, I.; Champion, R.; Madkhaly, S.; Morley, C.; O'Shea, J.; Evans, W.; Saint, R.; et al. Additively manufactured ultra-high vacuum chamber for portable quantum technologies. *Addit. Manuf.* **2021**, *40*, 101898. [[CrossRef](#)]
35. Mohamed, A.E.M.A.; Sheridan, R.; Bongs, K.; Attallah, M.M. Microstructure-magnetic shielding development in additively manufactured Ni-Fe-Mo soft magnet alloy in the as fabricated and post-processed conditions. *J. Alloys Compd.* **2021**, *884*, 161112. [[CrossRef](#)]
36. Madkhaly, S.; Coles, L.; Morley, C.; Colquhoun, C.; Fromhold, T.; Cooper, N.; Hackermüller, L. Performance-Optimized Components for Quantum Technologies via Additive Manufacturing. *PRX Quantum* **2021**, *2*, 030326. [[CrossRef](#)]
37. Ravenhall, S.; Yuen, B.; Foot, C. High-flux, adjustable, compact cold-atom source. *Opt. Express* **2021**, *29*, 21143–21159. [[CrossRef](#)]
38. Rushton, J.A.; Aldous, M.; Himsforth, M.D. Contributed Review: The feasibility of a fully miniaturized magneto-optical trap for portable ultracold quantum technology. *Rev. Sci. Instrum.* **2014**, *85*, 121501. [[CrossRef](#)]
39. Burrow, O.S.; Osborn, P.F.; Boughton, E.; Mirando, F.; Burt, D.P.; Griffin, P.F.; Arnold, A.S.; Riis, E. Stand-alone vacuum cell for compact ultracold quantum technologies. *Appl. Phys. Lett.* **2021**, *119*, 124002. [[CrossRef](#)]
40. Little, B.J.; Hoth, G.W.; Christensen, J.; Walker, C.; De Smet, D.J.; Biedermann, G.W.; Lee, J.; Schwindt, P.D.D. A passively pumped vacuum package sustaining cold atoms for more than 200 days. *AVS Quantum Sci.* **2021**, *3*, 035001. [[CrossRef](#)]
41. Cherubini, A.; Papini, A.; Vertechy, R.; Fontana, M. Airborne Wind Energy Systems: A review of the technologies. *Renew. Sust. Energ. Rev.* **2015**, *51*, 1461–1476. [[CrossRef](#)]
42. Feng, Y.; Zhang, C.; Baek, S.; Rawashdeh, S.; Mohammadi, A. Autonomous Landing of a UAV on a Moving Platform Using Model Predictive Control. *Drones* **2018**, *2*, 34. [[CrossRef](#)]
43. Boaz, B. Power Line Charging Mechanism for Drones. *Drones* **2021**, *5*, 108. [[CrossRef](#)]
44. Sri, K.R.B.; Aneesh, P.; Bhanu, K.; Natarajan, M. Design Analysis of Solar-Powered Unmanned Aerial Vehicle. *J. Aerosp. Technol. Manag.* **2016**, *8*, 397–407. [[CrossRef](#)]
45. Grepow.com. Available online: <https://www.grepow.com/page/high-voltage-battery.html> (accessed on 6 December 2021).